RSC Advances

ROYAL SOCIETY OF CHEMISTRY

www.rsc.org/advances

Tunable Sound Absorption of Silicone Rubber Materials *via* Mesoporous Silica

Yong Huang,[†‡] Dong Zhou,[†] Yunchuan Xie[§], Jianye Yang[‡] and Jie Kong*[†]

[†]MOE Key Laboratory of Space Applied Physics and Chemistry, Shaanxi Key Laboratory of Macromolecular Science and Technology, Department of Applied Chemistry, School of Science, Northwestern Polytechnical University, Xi'an, 710072, P. R. China

[‡]College of Materials Science and Engineering, Xi'an University of Science and Technology, Xi′an, 710054, P. R. China

[§]Department of Applied Chemistry, School of Science, Xi'an Jiaotong University, Xi'an, 710049, P. R. China

Abstract: In this contribution, a new pathway for the regulation of sound absorption property of silicone rubber (SR) materials was presented using worm-like mesoporous silica (MS) with nanoscaled channels and pores. The MS enhanced the sound absorption coefficient of SR in a wide range of sound frequency from 1 to 5 kHz. By introducing the MS with an average pore diameter of 5.56 nm and a specific surface area of 1026 m^2 g^{-1}, the sound absorption coefficient of MS/SR composite was as high as 0.83 at a sound frequency of 1.8 kHz, which is nearly triple compared to the pure SR. Moreover, the mechanical and thermal properties of the SR were retained in the composite. The reflection and friction of sound wave between the pore walls and the depleted energy by viscous absorption were suggested as the main mechanism responsible for the enhanced sound absorption coefficient. It is helpful to design and fabricate rubber materials with tunable sound absorption property.

Keywords: *sound absorption, silicone rubber, mesoporous silica*

Introduction

Sound absorbing materials are passive mediums that decrease noise in products or environment. For various absorption materials such as resonance and porous absorption materials, the sound energy is mainly dissipated by heat conduction absorption, relaxation absorption, or viscous absorption.[1–4] For resonance absorption materials made of wood, fiber, rubber, or aluminum plate containing cavities between the layers, the sound energy gets converted into heat energy after dissipation. When the sound wave passes through the cavities, it causes the air to vibrate and converts shear wave into longitudinal wave resulting in the reduced and dissipated sound energy with a narrow and low frequency. In case of porous absorption materials, the sound energy is dissipated by viscous absorption of sound wave in a wide range of high frequency depending on the density of the medium. The high density of the polymer materials leads to lower viscous absorption of the sound wave compared to that in the air medium. Silicone rubber (SR) is an important elastomer material which is in general, stable, non-reactive and resistant to extreme environments and temperatures from −60 to 300 °C. SRs are extensively employed for the manufacture of automotives, electronics, and medical devices and implants [5–10] because of the above mentioned properties. However, the sound absorption property of bulk SR is not adequate for an efficient noise control, thus limiting its application for the production of mufflers of cars, air conditioner parts, pump chambers, and elevated roads.[11–13] Therefore, to enhance the sound absorption property of SR, the vermiculites or zeolites were used as sound absorption additives, however, the sound absorption could only be improved in a narrow acoustic frequency region.[14] Mesoporous silica (MS) materials possessing high surface area and uniform pore size exhibit significant

potential in catalysis, separation, absorption, bioreactors, and sensors.[15–19] The structural, morphological, and pore size control of MS materials have been extensively studied.[20–26] Therefore, the MS material with tunable pore size is potential to be employed as a promising candidate to enhance the sound absorption property of SR. In this study, the MS with various pore dimensions were synthesized and the effects on sound absorption properties of SR were investigated systematically.

Experimental Section

Materials

Tetraethylorthosilicate (TEOS) was purchased from National Medicine Co., Ltd (Shanghai, China). Cetyltrimethylammonium bromide (CTAB) was received from Lingfeng Chemical Reagent Co., Ltd (Shanghai, China). Ammonia was purchased from Paini Chemical Reagent Co., Ltd (Zhengzhou, China). Poly(methylvinylsiloxane) (Mn = 600,000 g mol^{-1}) was purchased from Zhonghao Chenguang Institute (Chengdu, China). Dicumyl peroxide (DCP) was purchased from Shanghai Jingchun Reagent Co., Ltd (Shanghai, China).

Synthesis of MS

TEOS was added with continuous stirring into a mixture of water and CTAB or water, ethanol and CTAB. After the self-assembly and hydrolysis, the system was further calcined at high temperature followed by the removal of the template resulting in the formation of MS. The detailed procedure is as follows: CTAB (1 g) was taken in a 250 mL flask containing water (120 mL). Clear mixture was obtained after vigorous stirring for 3 h. Subsequently, pH

of the clear mixture was adjusted to 9–10 using ammonia. TEOS (6 mL) was added drop-wise and the resulting mixture was kept at 40 °C for 20 h for hydrolysis, and the precipitates were formed. Then the precipitates were filtered and washed three times with distilled water followed by drying in vacuum at 60 °C. Finally, the dried powders were calcined at 550 °C for 5 h under an air atmosphere resulting in the formation of MS as white powder.

Synthesis of the MS/SR Composites

Poly(methylvinylsiloxane) (100 g), MS (3–10 g), the reinforcing agent of gasphase silica (10 g), and the cross-linking agent of DCP(2 g) were blended for 40 min on a two-roll mill. The MS/SR composite specimens were obtained by curing at 170 °C for 20 min and at 200 °C for 4 h.

Characterization

Fourier transform infrared spectroscopy (FT-IR) was conducted at room temperature on a Nicolet IS10 IR spectrometer in the range of 4000–500 cm^{-1} with a resolution of 2 cm^{-1} and 16 scans. The specimen was prepared by dispersing the powdered samples in KBr and compressing the mixture to form disks.

Scanning electron microscopy (SEM) images were obtained by a Philips XL30 electron microscope operating at 8.0 kV. Transmission electron microscope (TEM) images were recorded by a FEI Tecnai G2 F20 electron microscope operating at 100 kV.

Powder X-ray diffraction (XRD) measurement was performed on an X′Pert Pro Powder diffractometer from PANalytical (Cu Kα radiation, 40 kV, 40 mA) (PANalytical B.V., Netherlands). The X′Celerator Scientific RTMS detection unit was used as detector.

X-ray photoelectron spectroscopy (XPS) measurements were conducted on a Kα spectrometer (Thermo Fisher Scientific, Waltham, MA, USA), and the core level spectra were measured using a monochromatic Al KR X-ray source.

The surface areas, pore volumes, and pore size distribution were determined by Nitrogen (N_2) adsorption–desorption isotherms using a Nova 2200E instrument, by employing the Brunauer–Emmett–Teller (BET) equation for surface area calculation, and the Barrett–Joyner–Halenda (BJH) method for pore size analysis. The desorption branches of the isotherm obtained experimentally were used for the analysis.

Thermogravimetric analysis (TGA) was performed using a simultaneous thermoanalyzer STA 449 F3 coupled with a quadrupole mass spectrometer QMS 403 C Aeolos (Netzsch Group, Germany) at a temperature range between 40 and 1000 °C, with a heating rate of 10 K min^{-1} under an argon atmosphere (gas flow: 50 mL min^{-1}).

Sound absorption coefficient was tested by AWA1622 standing wave tube. Room temperature tensile testing of the composites was done following GB/T528-1998 on an Instron1211

testing machine at a crosshead speed of 500 mm min^{-1}. The measurement was performed on five test samples and the middle value was selected. Hardness (shore A) of the composites was determined on a hardness testing machine according to the standard of GB/T531-1999 of China.

Results and Discussion

Synthesis of MS with tunable pores

The MS was synthesized using TEOS as a hydrolyzable inorganic precursor and CTAB as template as illustrated in **Scheme 1**.[27] The two-step self-assembly led to stable hybrid micelles, followed by catalyst-induced silica condensation in a pH range of 9–10. The silica condensation was further initiated by the addition of ammonia as catalyst. Finally, they were condensed to form silica precursor on the surface of micelles. **Figure** 1 illustrates the FT-IR spectra of MS-1 and MS-3 exhibiting obvious peaks at 805, 1081, 1652, and 3428 cm^{-1} corresponding to Si–O–Si symmetric and asymmetric stretching, water molecules retained by siliceous materials and –OH stretching, respectively.[28,29] After calcination, the density of silanol groups distributed on the surface of mesoporous silica at 3737 cm^{-1} was reduced. The absorption peaks at 2950–2850 and 1500 cm^{-1} are attributed to C–H stretching and C–H bending in the CTAB precursor. After calcination, all the above mentioned peaks disappeared from the precursor, indicating a complete removal of CTAB after the formation of MS.

The MS with tunable pores were prepared by regulating the reaction parameter as listed in **Table 1.** Their characteristics SEM images are shown in **Figure 2**. The uniform nanoparticles and clusters with a dimension of 50–80 nm were observed for MS samples (MS-1–MS-4) and

the TEM confirmed their mesoporous structures. **Figure 3** displays the worm-like elliptic particles with approximate diameter of nanopores as 4 nm. A high age temperature during calcination results in the smaller worm-like elliptic particles without any change in the bulk dimension as presented in **Figure 3d** indicating that the pore dimension is dependent on the size of micelles, which was decided by the mole ratio of TEOS to CTAB, the temperature, and the dispersion. Moreover, MS-5 consisted of elliptic particles with a larger particle size of 400–600 nm, however, the mesopores or channels could not be observed in the TEM image (**Figure 4**). This was attributed to the addition of co-solvent of ethanol which decreased the polarity of the solution and reduced the self-assembly during formation of silica.

N_2 Adsorption–desorption isotherm of MS

Figures 5a-c show the N_2 adsorption–desorption isotherms of MS prepared using different mole ratios of TEOS to CTAB. The samples MS-1, MS-2, and MS-3 exhibit a combination of isotherms II and IV with a sharp inflection at a relative pressure P/P^0 of 0.2–0.3 indicating a capillary condensation inside the uniform mesopores. The above mentioned phenomenon is a typical adsorption behavior of mesoporous materials. Moreover, the samples displayed a capillary condensation of N_2 at a high relative pressure ($P/P^0 > 0.9$) and a characteristic of high textural porosity.[30] The mesopore size distribution can be calculated by using the N_2 metastable adsorption branch kernels as listed in **Table 2**. For MS-1, MS-2, and MS-3, the specific surface area and pore volume increased from 806 to 1026 $m^2\ g^{-1}$ and from 0.85 to 1.43 $cm^3\ g^{-1}$, respectively, with a decrease in mole ratio of TEOS to CTAB. Consequently, the average pore diameter increased from 4.2 to 5.6 nm. The dense structure of MS-5,

different from the other MS samples, was also confirmed by the N_2 adsorption isotherm in **Figure 5d** exhibiting a type I isotherm where a sharp increase in adsorption was observed at a low relative pressure ($P/P^0 < 0.2$) because of adsorption of micropores. The specific surface area (BET) was about 808 m^2 g^{-1} and the average pore size of 1.87 nm measured from BJH analysis.

Analyses of XRD and XPS of MS

The powder XRD patterns in **Figure 6** elucidate fine phase structures of the MS. The broad peak at 2θ = 23.5° is indexed as the silica with amorphous structure. Moreover, the three peaks at 2θ = 43.9, 64.4, and 77.5° are indexed as [222], [422], and [023] crystal face, respectively, of the orientated silica crystals in amorphous silica matrix (ICDD data file 76-1390, 80-2157). The XPS analyses in **Figure 7** show the existence of silicon, oxygen, and carbon elements in the MS. The silicon dioxide with Si2p binding energy (BE) of 103.8 eV and O1s BE of 533.1 eV are detected.[31] The BE of C1s XPS peak is determined to be 284.6 eV corresponding to the free carbons, which come from the template carbide because of unsufficient oxidation. At about 286.2 eV, a slight broadening in the peak is attributed to surface oxygen groups with single bonds.[32] The BE of the O1s and Si2p XPS peaks is determined to be equal to 534.8 and 105.2 eV, respectively, and the two peaks are considered to be derived from Si–OH, thus, verifying the presence of Si–OH on the surface of the MS. [33] Moreover, the N_2 and bromine were not detected because N1s and Br3d peaks could not be observed, indicating that the template of CTAB had been removed, which was in correspondence with the result from the FT-IR analysis.

Sound Absorption of MS/SR Composites

The sound absorption coefficient (α) of the MS/SR composites was measured according to the standard of ISO10534-213, which is defined as the ratio of the acoustic energy absorbed $\prod_{diss}$ to the acoustic energy incident $\prod_{in}$ on the surface as shown in Eq. 1.[34]

$$\alpha = \frac{\prod_{diss}}{\prod_{in}} = \frac{\prod_s + \prod_v + \prod_t}{s[p_0]^2 / 2\rho_0 c_0} \text{.....(1)}$$

Where $\prod_{diss}$ is the sum of the powers dissipated by structural damping $\prod_s$, viscous $\prod_v$, and thermal effect $\prod_t$, ρ_0 is the density of the interstitial fluid and p is the interstitial pressure of the porous-elastic medium. The method for the calculation of sound absorption coefficient from the material's Biot properties was reported in the literature.[35] The sound absorption coefficient was calculated as the average value of five cylindrical pieces over the frequency range of 100 to 6300 Hz. **Figure 8** demonstrates the dependence of sound absorption coefficient on frequency for MS/SR composites**.**

First, the sound absorption coefficient of the MS/SR composites is strongly dependent on the sound frequency. The II-a and II-b zones in **Figure 8,** displaying the frequency range between 1 and 5 kHz, demonstrate the significant enhancement in the sound absorption coefficient of the MS-1–MS-3/SR composites. In contrast, in the low frequency zone (I) and the high frequency zone (III), the addition of MS has no obvious influence on the sound absorption property of SR because of mismatching of the pore dimension of MS and the sound wave. Second, the mesoporous structures of MS significantly influence the enhanced efficiency of the MS/SR composites. When the pore diameter and specific surface area of MS is increased

from 4.23 to 5.56 nm and from 806 to 1026 m^2 g^{-1}, respectively, the enhanced efficiency is further increased. The sound absorption coefficient of MS-3/SR is as high as 0.83 at a sound frequency of 1.8 kHz, which is nearly triple compared to the pure SR. In contrast, MS-5 does not demonstrate any effect on the sound absorption of the MS/SR composites because of the ultralow pore diameter of 1.87 nm and pore volume of 0.38 cm^3 g^{-1}.[11,14] Third, the synergistic effect of frequency and mesoporous structure on sound absorption coefficient can be easily obtained. For MS-3 with a large pore diameter and volume, the maximum sound absorption coefficient was obtained at 1.8 kHz. When the pore diameter and volume were decreased, the maximum sound absorption coefficient was obtained at a high frequency range of 3.2–4.0 kHz. In the high frequency zone (II-b in **Figure 8**), MS-1 and MS-2 with a medium pore diameter and volume exhibit significant sound absorption property.

Furthermore, the average sound absorption coefficient, defined as the average value of sound absorption coefficient at 125, 250, 500 Hz, 1, 2 and 4 kHz, can be used to evaluate the sound absorption property in practical application. One material can be considered as a sound-absorption material if its average value of the sound absorption coefficient is more than 0.2[38]. For the pure SR, the average sound absorption coefficient was determined to be 0.26. However, for the MS/SR composites, the average sound absorption coefficient was in the range of 0.39 and 0.42. Therefore, the MS/SR composites are potential in the material candidates for lowering the noise level of industrial products.

In this study, the enhanced mechanism of sound absorption coefficient after the addition of

MS is suggested in **Scheme 2**. When a sound wave diffuses on the surface of the MS/SR composite, the channels in the worm-like mesoporous particles of MS dispersed in SR matrix are vertical, parallel or oblique to the incident direction of sound wave. When the channels of MS are vertical to the incident direction of the sound wave, the reflection and transmission lead to the air vibration and friction between the pore walls and sound wave resulting in the depleted energy as presented in **Scheme 2b**. When the channels of MS are parallel to the incident direction of the sound wave, the sound wave causes air flow and sound energy gets dissipated by viscous loss as shown in **Scheme 2d**. Moreover, the sound wave leads to the friction between the pore walls and the sound energy is consumed as heat.[36–37] When the channels of MS are oblique to the incident direction of the sound wave, the depleted sound energy exhibits dependence on both the viscous and heat effect. Therefore, **Scheme 2f** illustrates that when the sound waves are reflected constantly, their travel path gets extended, thus, causing the interaction between the air and the pore walls. Importantly, the consumption of sound energy in all the three abovementioned cases explained the enhanced mechanism of sound absorption coefficient after the addition of MS.

To obtain the best addition amount of MS in the composites, the dependence of sound absorption coefficient on the sound frequency for the MS/SR composites with various content of MS-3 is presented in **Figure 9**. The addition amount of MS has an insignificant influence on sound absorption coefficient between large frequencies ranging from 0.4 to 6.5 kHz, indicating that even less amount of the added MS can effectively improve the sound absorption property of SR. Thus, a low amount of MS added to SR gives an opportunity to

obtain the cost-effective MS/SR composites with maximum sound absorption property.

The Mechanical and Thermal Properties of the MS/SR Composites

The mechanical properties including tensile strength, elongation at break, and hardness of the MS/SR composites are listed in **Table 3**. The results indicated that the addition of MS with suitable pore size and specific surface area, to the pure SR, did not reduce the tensile strength, elongation at break, and hardness. In another word, the MS with suitable pore size and volume enhanced the sound absorption property of SR without reducing its mechanical properties.

The TGA coupled with mass spectrometry was employed to study the thermal property and pyrolysis behavior of the MS/SR composites under high temperature. The investigation of the TGA curves shown in **Figure 10** reveals a rapid thermolytic degradation of all the samples of the composites in the temperature range of 450–720 °C, followed by the levelling off of the TGA curve. The char yield at 720 °C was in the range of 17–21% according to the content of MS-3 in the composites, which was higher than the char yield of 13% of the pure SR. **Figure 11** demonstrates the thermograms of the MS/SR composite obtained from the simultaneous TGA and mass spectrometry analysis indicating that the thermolysis of MS-3/SR is mainly accompanied with the evolution of H_2 (m/z = 2), C (m/z = 12), hydrocarbons CH_2 (m/z = 14), CH_4 (m/z = 16), CHCH (m/z = 26), CH_2CH_2 (m/z = 28), CH_2CH_3 (m/z = 29), CH_3CH_3 (m/z = 30), and oligomer fragments (m/z = 36), responsible for the thermolysis of Si–CH_3, Si–CH_2–CH_2– groups and the cleavage of C–C bonds over the temperature range of

450–720 °C.[39-40] According to the literatures,[41–46] the precipitated silica was damaged to the thermal resistance of SR. However, in this study, the results did not indicate the loss of the thermal-resistance due to MS because MS was calcined at 550 °C to remove almost all the hydroxyl group residues.

Conclusions

In this study, the MS with tunable pores were synthesized using TEOS as precursor and CTAB as template. The worm-like MS with nano channels enhanced the sound absorption coefficient of SR in a wide range of sound frequency. The dependence of enhancement in sound absorption coefficient on frequency was in accordance with the pore size and structures of MS. For the MS-3/SR composite with a pore diameter and specific surface area of 5.56 nm and 1026 m^2 g^{-1}, respectively, the sound absorption coefficient was as high as 0.83 at sound frequency of 1.8 kHz, which is nearly triple than the pure SR. Moreover, the mechanical and thermal properties of the SR were retained in the composite. The sound wave reflection and friction between the pore walls and the depleted energy by viscous absorption were suggested as the main mechanism for the enhanced sound absorption coefficient after the addition of MS into SR materials. This study provides a significant pathway for the design and fabrication of cost-effective soft materials with tunable sound absorption property.

Associated Content

Author Information

***Corresponding Author**

E-mail: kongjie@nwpu.edu.cn. Tel (fax): +86-29-88431621.

Notes

The authors declare no competing financial interest.

Acknowledgments

This study was supported by the Natural Science Foundation of China (No. 21174112). J.K. acknowledges the support from the Program for New Century Excellent Talents of Education Ministry of China (NCET-11-0817) and the Basic Scientific Research Foundation of Northwestern Polytechnical University.

References

(1) Zhou, H.; Li, B.; Huang, G.; He, J. S. *J. Sound Vib.* **2007**, 304, 400-406.

(2) Lu, T. J.; Hess, A.; Ashby, M. F. *J. Appl. Phys.* **1999**, 85, 7528-7539.

(3) Howe, M. S. *J. Sound Vib.* **1980**, 70, 407-411.

(4) Crocker, M. J.; Price, A. J. *J. Sound Vib.* **1969**, 9, 469-486.

(5) Wang, X. L.; Dou, W. Q. *Thermochimica Acta* **2012**, 529, 25-28.

(6) Meunier, L.; Chagnon, G.; Favier, D.; Orgeas, L.; Vacher, P. *Polym. Test.* **2008**, 27, 765-777.

(7) Di, M. W.; He, S. Y.; Li, R. Q.; Yang, D. Z. Nuclear Instruments and Methods in Physics Research Section B: Beam Interactions with Materials and Atoms. **2006**, 252, 212-218.

(8) Thomas, S.; Stephen, R. Singapore. Rubber Nanocomposites: Preparation, Properties and Application. John Wiley & Sons (Asia) Pte Ltd, **2010**.

(9) Malas, A.; Das, C. K.; Das, A.; Heinrich, G. *Mater. Des.* **2012**, 39, 410-417.

(10) Katihabwa, A.; Wang, W. C.; Jiang, Y. *J. Reinf. Plast. Comp.* **2011**, 30, 1007–1014.

(11) Ashby, M. F.; Lu, T. *J. Sci. China Ser. B.* **2003**, 46, 521–32.

(12) Gibson, L. J.; Ashby, M. F. Cellular Solids: Structure and Properties. Cambridge

University Press, **1999**.

(13) Dazel, O.; Becot, F. X.; Jaouen, L. *Acta Acustica. United Ac.* **2012**, 98, 567-576.

(14) Duan, C. Y.; Cui, G.; Xu, X. B.; Liu, P. S. *Appl. Acoust.* **2012**, 73, 865-871.

(15) Lin, N.; Yang, J. Y.; Wu, Z. Y. *Micropor. Mesopor. Mater.* **2011**, 139, 130-137.

(16) Nowak, I.; Ziolek, M.; Jaroniec, M. *J. Phys. Chem. B* **2004,** 108, 3722-3727.

(17) Wu, Z.Y.; Wang, H. J.; Zhuang, T. T.; Sun, L. B.; Wang, Y. M.; Zhu, J. H. *Adv. Funct. Mater.* **2008**, 18, 82-94.

(18) Choi, M.; Heo, W.; Kleitz, F.; Ryoo, R. *Chem. Commun.* **2003,** 1340-1341.

(19) Beck, J. S.; Vartuli, J. C.; Roth, W. J.; Leonowicz, M. E.; Kresge, C. T.; Schmitt, K. D.; Olson, D. H.; Sheppard, E. W. *J. Am. Chem. Soc.* **1992,** 114, 10834–10843.

(20) Qiao, S. Z.; Bhatia, S. K.; Nicholson, D. *Langmuir* **2004**, 20, 389-395.

(21) Trens, P.; Tanchoux, N.; Maldonado, D.; Galarneau, A.; Renzo, D. F.; Fajula, F. *New. J. Chem.* **2004,** 28, 874-879.

(22) Lee, J. W.; Shim, W. G.; Yang, M. S.; Moon. H. *J. Chem. Eng. Data* **2004,** 49**,** 502-509.

(23) Tanchoux, N.; Trens, P.; Maldonado, D.; Renzo, F. D.; Fajula, F. *Coll. Surf. A* **2004**, 246, 1-8.

(24) Trens, P.; Tanchoux, N.; Papineschi, P. M.; Maldonado, D.; Renzo, F. D.; Fajula, F. *Micropor. Mesopor. Mater.* **2005**, 86, 354-363.

(25) Pariente, S.; Papineschi, P. M.; Trens, P. *Coll. Surf. A* **2007**, 300, 216-221.

(26) Russo, P. A.; Ribeiro, M. L.; Carrott, R. P.; Carrott, J. M. *Adsorption* **2008**, 14, 367-375.

(27) Climent, E.; Martínez, R.; Sancenón, F.; Marcos, M. D.; Soto, J.; Maquieira, A.; Amorós, P. *Angew. Chem. Int. Ed.* **2010**, 49, 7281–7283.

(28) Kłonkowski, A. M.; Widernik, T.; Grobelna, B.; Jozwiak, W. K.; Proga, H.; Szubiakiewicz, E. *J. Sol-Gel. Sci. Technol.* **2001**, 20, 161–180.

(29) Singh, L. P.; Agarwal, S. K.; Bhattacharyya, S. K.; Sharma, U.; Ahalawat, S. *Nanomater. Nanotech.* **2011**, 1, 44–51.

(30) Zhao, Q. C.; Chen, W. M.; Zhu, Q. R. *Nanotechnology* **2004**, 15, 958–961.

(31) Kong, J.; Kong, M. M.; Zhang, X. F.; Chen, L. X.; An, L. N. *ACS Appl. Mater. Interfaces* **2013**, 5, 10367−10375.

(32) Paparazzo, E. *Surf. Interface Anal.* **1996**, 24, 729-730.

(33) Lu, F.; Wu, S. H.; Hung, Y.; Mou, C. Y. *Small* **2009**, 5, 1408–1413.

(34) Sgard, F.; Castel, F.; Atalla, N. *Appl. Acoust.* **2011**, 72, 157-168.

(35) Allard, J. F.; Atalla, N. Propagation of Sound in Porous Media: Modelling Sound Absorbing Materials. John Wiley & Sons, **2009**.

(36) Zhou, H.; Li, B.; Huang, G. S. *Mater. Lett.* **2006**, 60, 3451–3456.

(37) Zhou, H.; Li, B.; Huang, G. S. J. *Appl. Polym. Sci.* **2006**, 101, 2675–2679.

(38) Liu, J. L.; Wei, B.; Lei, S.; Zuo, B. Q.; Gao, W. D. *Appl. Acoust.* **2014**, 76, 128-137.

(39) Zhang, X. F.; Chen, L. X.; Meng, L. L.; Chen, F. F.; Kong, J. *Ceram. Int.* **2014**, 40: 6937-6947.

(40) Kong, J.; Schmalz, T.; Motz, G.; Müller, A. H. E. *J. Mater. Chem. C* **2013**, 1: 1507-1514.

(41) Timothy, A. O.; Walter, H. W. *Rubber Chem. Technol.* **1995**, 68, 59-76.

(42) Jesionowski, T. *J. Mater. Process.Tech.* **2008**, 203, 121-128.

(43) Shim, S. E.; Isayew, A. I. *Rubber Chem. Technol.* **2001**, 74, 303-316.

(44) Prasertsri, S.; Rattanasom, N. *Polym. Test.* **2012**, 31, 593-605.

(45) Taikum, O.; Friehmelt, R.; Scholz, M. *Rubber World* **2010**, 242, 35-44.

(46) Diao, S.; Zhang, S,; Yang, Z.; Feng, S.; Zhang, C.; Wang, Z.; Wang, G. *J. Appl. Polym. Sci.* **2011**, 120, 2440-2447.

Tables Captions

Table 1 Conditions used for the preparation of MS

Table 2 The physical parameters of MS determined by N_2 adsorption isotherm

Table 3 The mechanical properties of MS/SR composites

Table 1 Conditions used for the preparation of MS

Samples	Water:Ethanol:TEOS:CTAB mole ratio	Reaction conditions	Aged conditions
MS-1	2470:0:10:1	40 °C × 20 h	40 °C × 24 h
MS-2	4940:0:20:1	40 °C × 20 h	40 °C × 24 h
MS-3	2470:0:5:1	40 °C × 20 h	40 °C × 24 h
MS-4	2470:0:10:1	40 °C × 20 h	80 °C × 24 h
MS-5	1440:320:10:1	40 °C × 20 h	40 °C × 24 h

Table 2 The physical parameters of MS determined by N_2 adsorption isotherm

Samples	Specific surface area	Pore diameter	Pore volume	Wall thickness
	$m^2\ g^{-1}$	nm	$cm^3\ g^{-1}$	nm
MS-1	946	4.28	1.01	4.21
MS-2	806	4.23	0.85	4.22
MS-3	1026	5.56	1.43	4.21
MS-4	615	5.00	0.77	4.21
MS-5	808	1.87	0.38	4.25

Table 3 The mechanical properties of MS/SR composites

Samples	Tensile strength (MPa)	Elongation (%)	Hardness (shore A)
SR	1.42	196.8	26
MS-1/SR	1.44	169.7	27
MS-2/SR	1.43	161.4	27
MS-3/SR	1.55	184.9	28
MS-5/SR	2.05	166.3	32

Graphic Captions

Scheme 1 The schematic route for the formation of MS using TEOS as precursor and CTAB as template

Scheme 2 The suggested mechanism of enhanced sound absorption coefficient of SR after the addition of MS, (a) the channels of MS are vertical to the incident direction of the sound wave, (b) sound wave reflection and transmission, (c) the channels of MS are parallel to the incident direction of the sound wave, (d) sound wave reflection and transmission, (e) the channels of MS are oblique to the incident direction of the sound wave, and (f) sound wave reflection and transmission

Figure 1 FT-IR Spectra of MS-1 and MS-3 (a), (c) before calcination and (b), (d) after calcination

Figure 2 SEM images of (a) MS-1, (b) MS-2, (c) MS-3, and (d) MS-4

Figure 3 TEM images of (a) MS-1, (b) inserted local image of a, (c) MS-3, and (d) MS-4

Figure 4 Morphology of MS-5 formed in water/ethanol mixture at 40 °C, (a) SEM image and (b) TEM image

Figure 5 N_2 absorption–desorption isotherm and the inserted, corresponding pore-size distribution calculated using the absorption branch of the BET and BJH algorithm, respectively, for (a) MS-1, (b) MS-2, (c) MS-3, and (d) MS-5

Figure 6 XRD patterns of MS-1, MS-3, MS-4, and MS-5

Figure 7 XPS spectra of MS-1

Figure 8 The dependence of sound absorption coefficient on the sound frequency for MS-1, MS-2, MS-3, MS-5, and SR composites, (I) low frequency zone, (II) enhanced zone, and (III) high frequency zone

Figure 9 The dependence of sound absorption coefficient on the sound frequency for the MS-3/SR composites with various content of MS-3

Figure 10 Thermograms obtained from TGA under an argon atmosphere at a scanning rate of 10 K min^{-1} for MS/SR composites

Figure 11 Thermograms from simultaneous TGA and mass spectrometry analysis of the MS-3/SR composites with 5phr MS-3, (a) simultaneous thermalgravimetry (dashed lines) and mass spectrometry analysis with the evolution of species with m/z = 2, 14, 16, 28 and 36, (b) mass spectrometry analysis with the evolution of species with m/z = 12, 26, 29 and 30

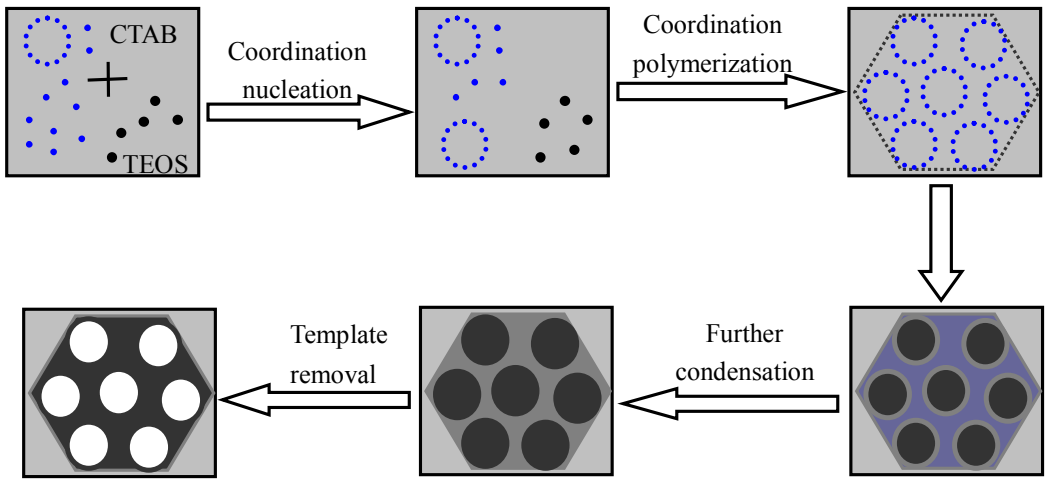

Scheme 1 The schematic route for the formation of MS using TEOS as precursor and CTAB as template

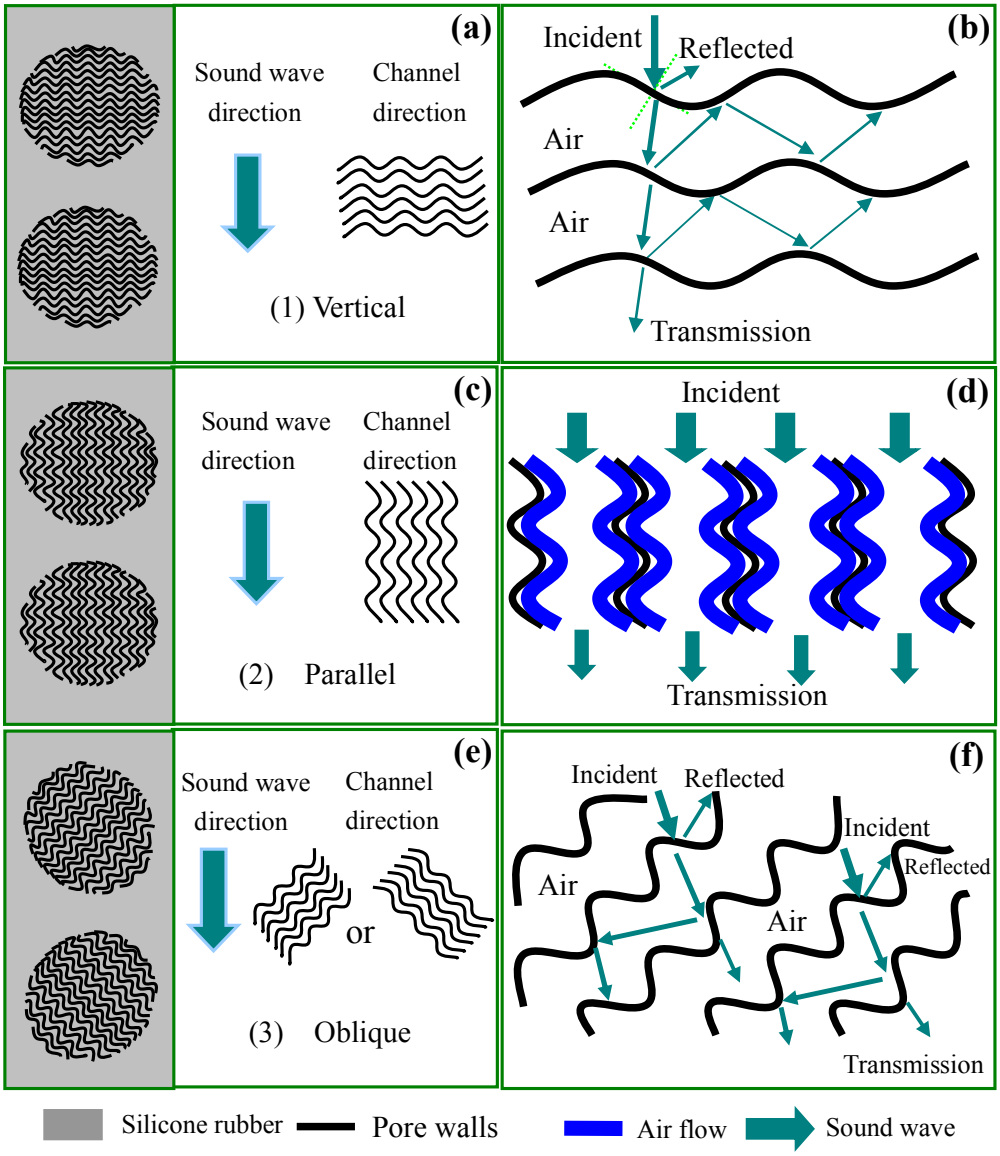

Scheme 2 The suggested mechanism of enhanced sound absorption coefficient of SR after the addition of MS, (a) the channels of MS are vertical to the incident direction of the sound wave, (b) sound wave reflection and transmission, (c) the channels of MS are parallel to the incident direction of the sound wave, (d) sound wave reflection and transmission, (e) the channels of MS are oblique to the incident direction of the sound wave, and (f) sound wave reflection and transmission

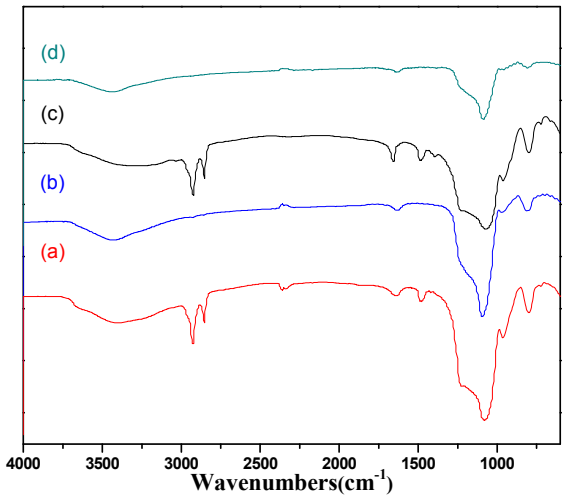

Figure 1 FT-IR Spectra of MS-1 and MS-3 (a), (c) before calcination and (b), (d) after calcination

.

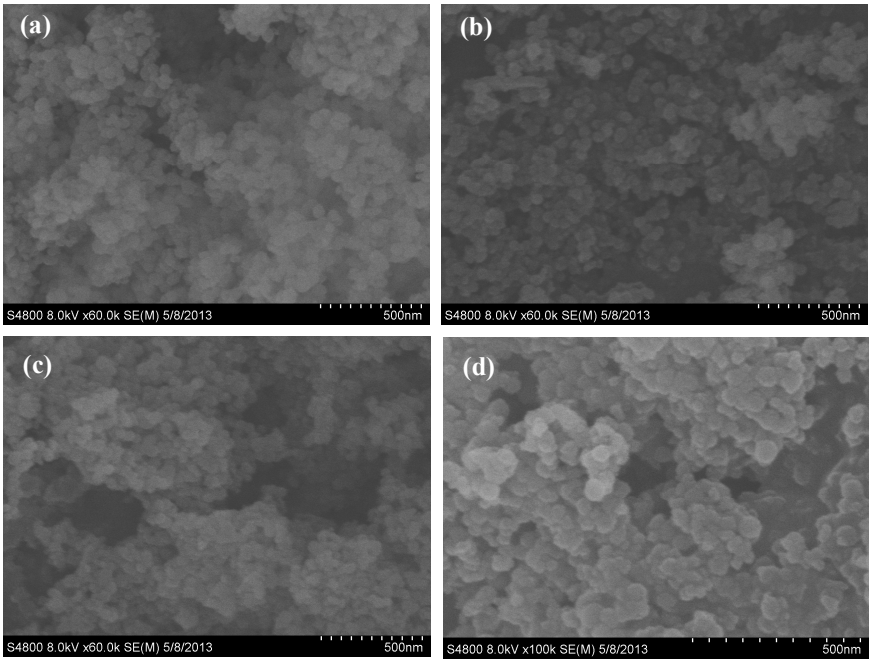

Figure 2 SEM images of (a) MS-1, (b) MS-2, (c) MS-3, and (d) MS-4

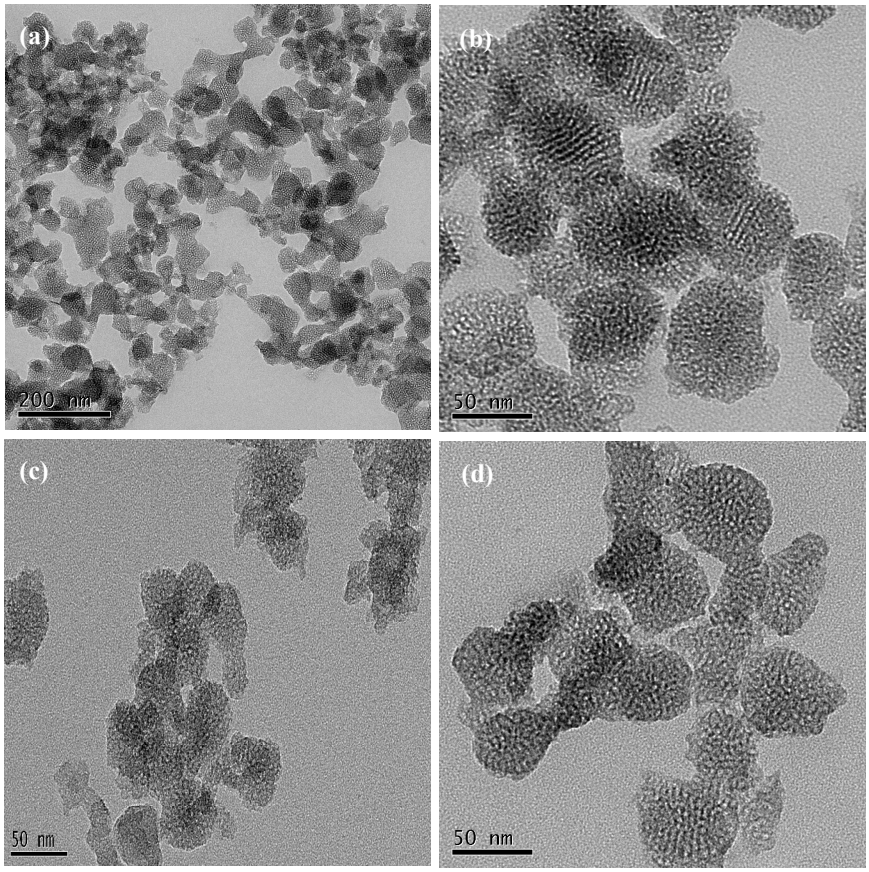

Figure 3 TEM images of (a) MS-1, (b) inserted local image of a, (c) MS-3 and (d) MS-4

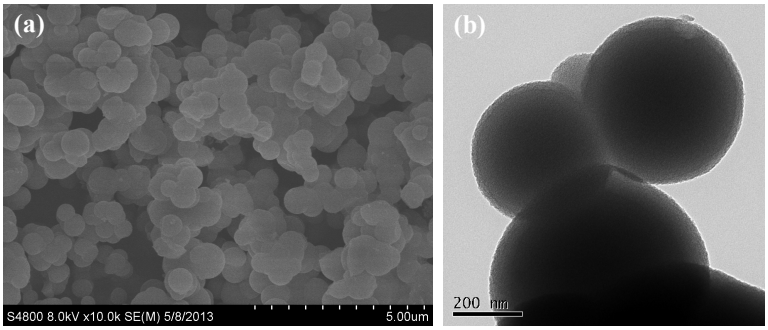

Figure 4 Morphology of MS-5 formed in water/ethanol mixture at 40 °C, (a) SEM and (b) TEM image

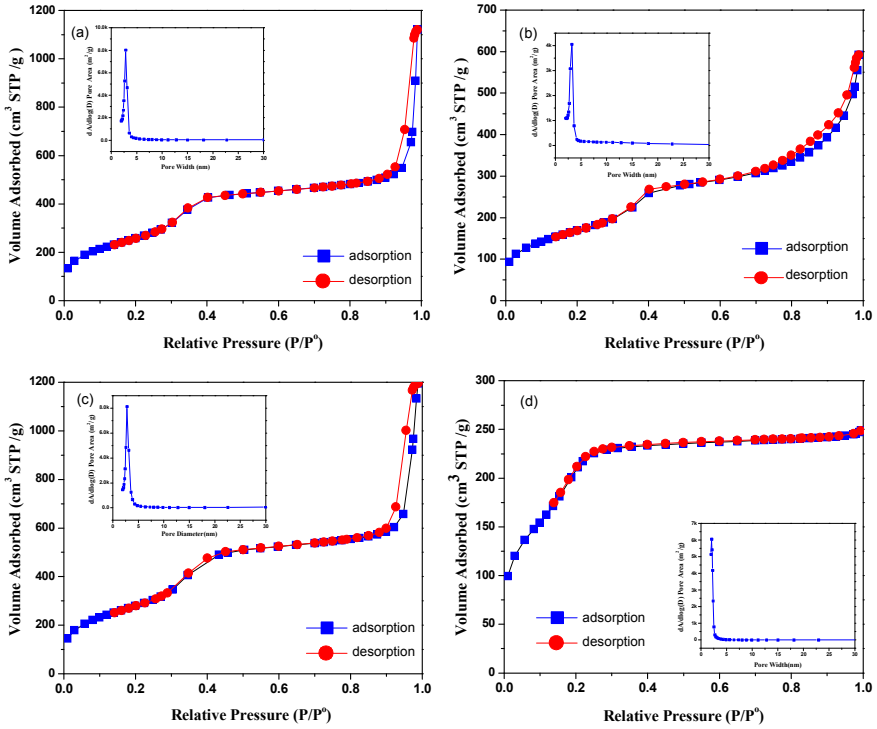

Figure 5 N_2 absorption–desorption isotherm and the inserted corresponding pore-size distribution calculated using the absorption branch of the BET and BJH algorithm, respectively, for (a) MS-1, (b) MS-2, (c) MS-3, and (d) MS-5

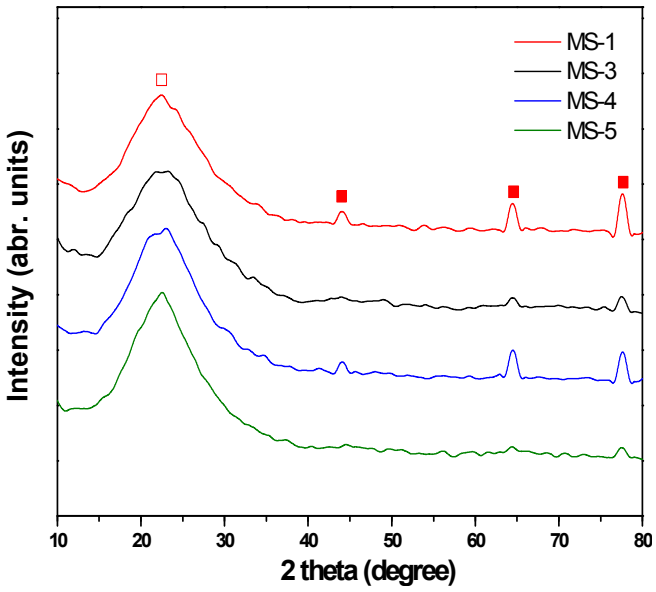

Figure 6 XRD patterns of MS-1, MS-3, MS-4, and MS-5.

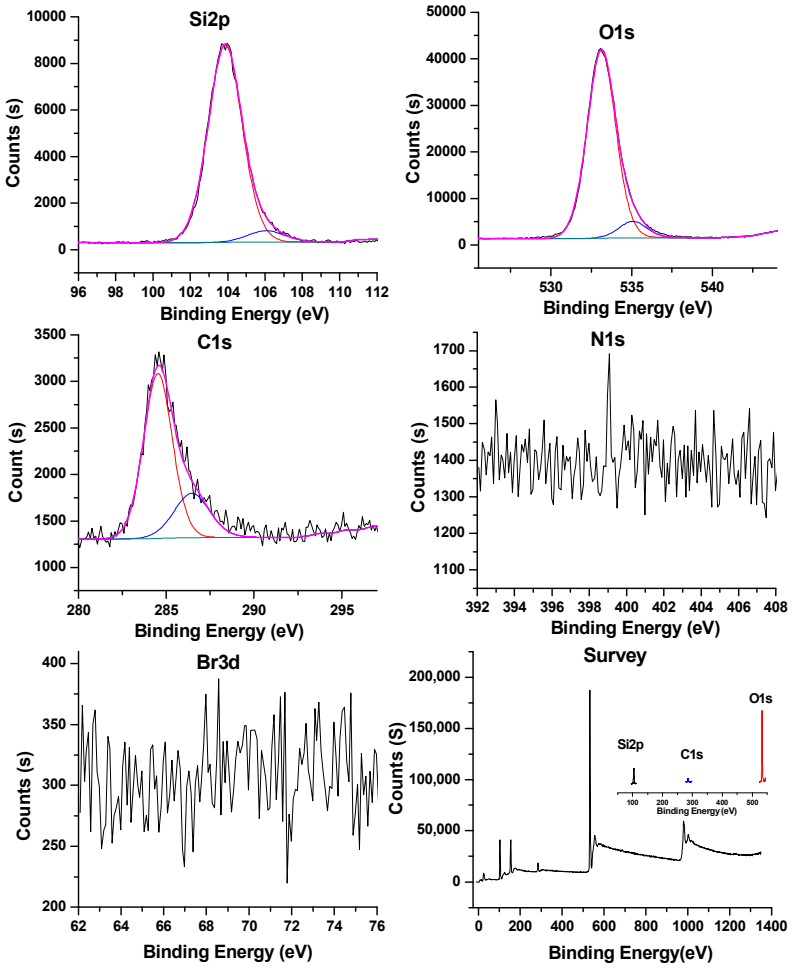

Figure 7 XPS spectra of MS-1

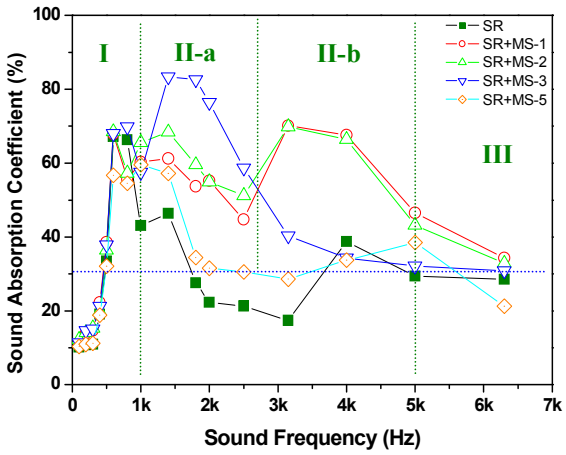

Figure 8 The dependence of sound absorption coefficient on the sound frequency for MS-1, MS-2, MS-3, MS-5, and SR composites, (I) low frequency zone, (II) enhanced zone, and (III) high frequency zone

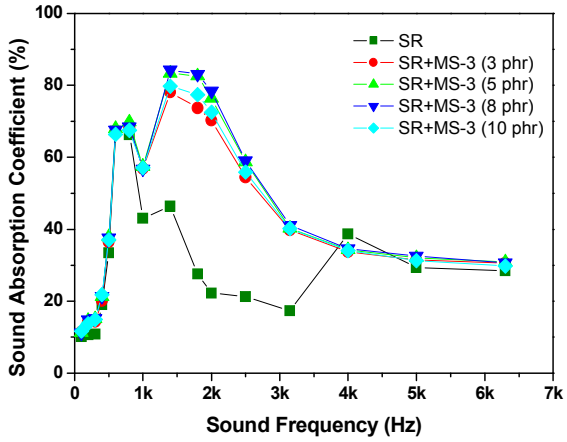

Figure 9 The dependence of sound absorption coefficient on the sound frequency for the MS-3/SR composites with various content of MS-3

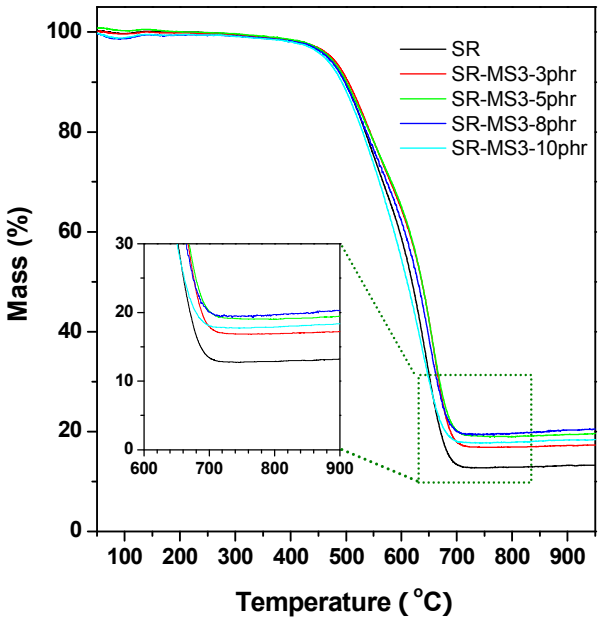

Figure 10 Thermograms obtained from TGA under an argon atmosphere at a scanning rate of 10 K min^{-1} for MS/SR composites

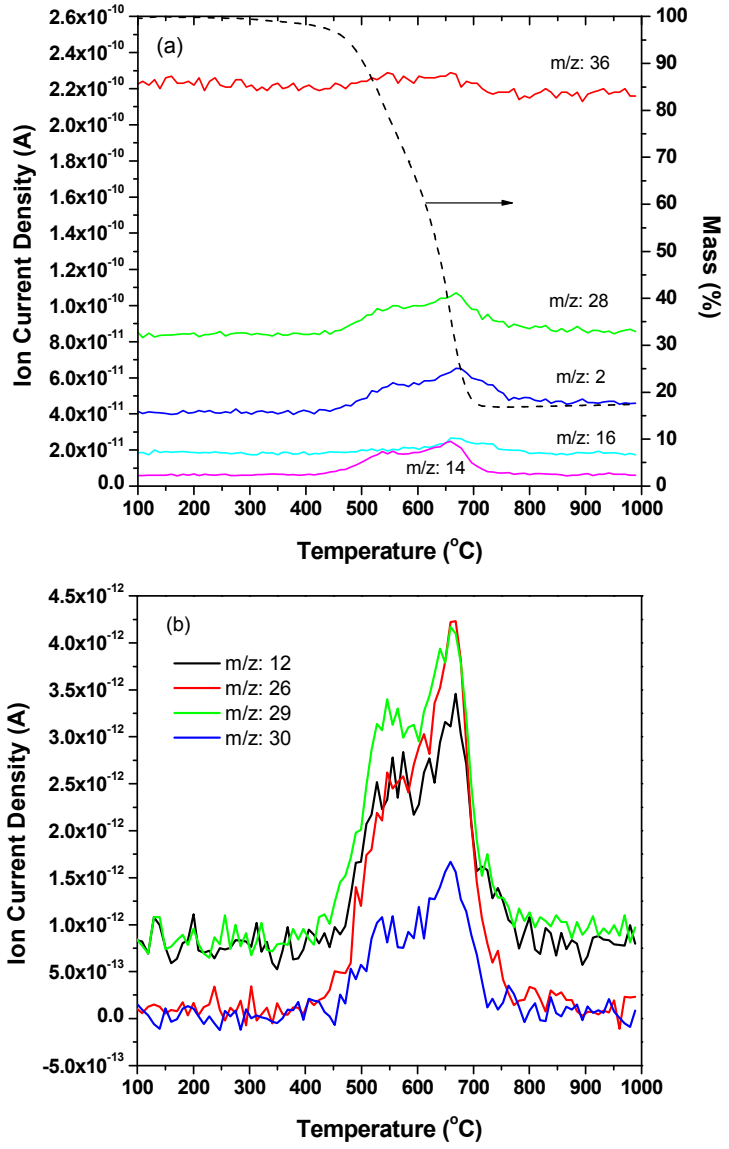

Figure 11 Thermograms from simultaneous TGA and mass spectrometry analysis of the MS-3/SR composites with 5phr MS-3, (a) simultaneous thermalgravimetry (dashed lines) and mass spectrometry analysis with the evolution of species with m/z = 2, 14, 16, 28 and 36, (b) mass spectrometry analysis with the evolution of species with m/z = 12, 26, 29 and 30

For Table of Contents Use Only

Tunable Sound Absorption of Silicone Rubber Materials with Mesoporous Silica

Yong Huang, Dong Zhou, Yunchuan Xie, Jianye Yang and Jie Kong*

Table of Contents Graphic:

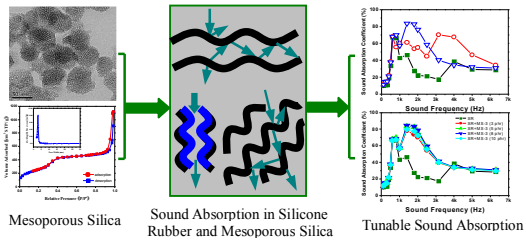

Mesoporous Silica | Sound Absorption in Silicone Rubber and Mesoporous Silica | Tunable Sound Absorption

One sentence highlights (20 words):

Mesoporous silica significantly enhanced sound absorption of silicone rubber via prolonging the propagation way and energy dissipated of acoustic wave.